*Electrochemical and Solid-State Letters*, **15** (5) A72-A75 (2012)
1099-0062/2012/15(5)/A72/4/$28.00 © The Electrochemical Society

# Intrinsic Surface Stability in $LiMn_{2-x}Ni_xO_{4-\delta}$ (x = 0.45, 0.5) High Voltage Spinel Materials for Lithium Ion Batteries

**Kyler J. Carroll,[a,*] Ming-Che Yang,[b] Gabriel M. Veith,[c,**] Nancy J. Dudney,[c,**] and Ying Shirley Meng[a,b,**,z]**

[a]*Department of NanoEngineering, University of California San Diego, La Jolla, California 92093-0448, USA*
[b]*Department of Materials Science and Engineering, University of Florida, Gainesville, Florida 32611-6400, USA*
[c]*Materials Science and Technology Division, Oak Ridge National Laboratory, Oak Ridge, Tennessee 37831, USA*

This work reports the surface stability of the high voltage Li ion cathode $LiMn_{2-x}Ni_xO_{4-\delta}$ (x = 0.5, 0.45) by comparing thin film and powder composite electrodes after cycling using X-ray photoelectron spectroscopy. The thin film electrodes offer the ability to probe the surface of the material without the need of a conductive agent and polymer binder typically used in composite electrodes. The results suggest that neither oxidation of $PF_6$ to $POF_3$ nor the decomposition of ethylene carbonate or dimethylene carbonate occurs on the surface of the spinel material. These results confirm the enhanced cycling stability and rate capability associated with the high voltage spinel material and suggests that the SEI layer forms due to the reaction of electrochemically inactive components in composite electrodes with the electrolyte.
 [DOI: 10.1149/2.008206esl] 

Manuscript submitted January 20, 2012; revised manuscript received February 20, 2012. Published March 12, 2012.

This work aims to explore the intrinsic surface stability of the high voltage $LiMn_{2-x}Ni_xO_{4-\delta}$ spinel-type cathodes. Research pertaining to this compound is growing because of its flat voltage plateau (4.7 V), excellent cycling stability (reversible capacity >135 mAh/g), good rate capability, and improved safety characteristics.[1] However, detailed information pertaining to the electrode/electrolyte interface still remains improperly investigated. A solid electrolyte interface (SEI) typically forms at the interface between the cathode and electrolyte region and originates from the oxidative decomposition of the electrolyte components at very high (>4.4 V) voltages. While the SEI layer can protect the electrode if stable, it also creates a barrier for lithium diffusion during electrochemical cycling and results in an increase in cell impedance and decreases the cycling efficiency.[2,3] Several groups have reported on the characterization of the SEI layer using composite electrodes containing conductive agents (carbon black) and polymeric binders (poly-vinylidene fluoride) and show the SEI consists of lithium alkyl carbonates ($ROCO_2$-Li), phosphates, LiF, and $Li_2CO_3$ originating from the electrolyte components.[4–15] However, these results are typically not a direct representation of the surface stability in the cathode material, rather a sum reaction of all the composite components, such as carbon black and poly-vinylidene fluoride (PVdF), which could react with the electrolyte at high voltages and accelerate the formation of the SEI layer.[16] Thin film electrodes offer the ability to investigate the intrinsic activity at the cathode surface, free of polymeric binders and conductive agents, while the controlled geometry enables more accurate measurements of ionic diffusion coefficients.[17] To adequately assess the intrinsic surface stability this work aims to compare both conventional powder composites and thin film electrodes after extended cycling.

## Experimental

*Synthesis of powders.*—Sol solutions were prepared from the stoichiometric mixtures of $Li(CH_3COO) \cdot 2H_2O$ (Fisher), $Ni(CH_3COO)_2 \cdot 4H_2O$ (Fisher), and $Mn(CH_3COO)_2 \cdot 4H_2O$ (Fisher) in distilled water. The solution was added drop-wise to a continuously stirred aqueous solution of citric acid. The pH of the mixed solution was adjusted to 6.5 by adding an ammonium hydroxide solution. The solution was then heated at 75°C overnight; a transparent gel was obtained. The resulting gel precursors were decomposed at 450°C for 10 hours in air and calcinated at 800°C for 10 hours.

*Synthesis of thin films.*—Before PLD deposition, a $LiMn_{2-x}Ni_xO_{4-\delta}$ (x = 0.45) target was synthesized by a solid-state reaction. Briefly, appropriate molar ratios of $MnO_2$, NiO and LiOH (Sigma-Aldrich) were mixed in a ball mill for 5 h. The mixture was then cold-pressed into a pellet and calcinated in air at 750°C for 24 h. After calcination, the pellet was ground and pressed into a pellet by a static press machine and subsequently fired in air at 900°C for 2 h to densify the target. To compensate the Li loss during the densification process and thin film deposition, extra Li was added in the target such that the Li to metal ratio is 1.3 in the starting material.

The $LiMn_{2-x}Ni_xO_{4-\delta}$ (x = 0.5) thin films were deposited on stainless steel (SS304) disks. A Lambda Physik KrF excimer laser with wavelength 248 nm was used in the deposition. Laser fluence and repetition rate were respectively controlled at 500 mJ and at 5Hz. Film depositions were carried out at a substrate temperature of 600°C in an oxygen partial pressure of 300 mTorr for 40 minutes and calcinated for an extra 20 minutes in oxygen-rich atmosphere. The thin films were subjected to a cooling rate of 10°C/min.

*Characterization.*—X-ray diffraction (XRD) data were collected using a Philips APD 3720 diffractometer using a Cu Kα radiation source operated at 45 kV and 20 mA. The scan speed was 3 sec/step with a step size of 0.02 degrees two theta. Images were collected using a field emission scanning electron microscopy (FEG-SEM, JEOL JSM-6335F) with an accelerating voltage of 15 kV. X-ray photoelectron spectroscopy data were collected using a PHI 3056 spectrometer equipped with a hemispherical detector, 54.7 degrees off normal, with a Mg anode source operated at 15 kV and an applied power of 350 W. The chamber pressure was kept at $<10^{-8}$ Torr during the measurements. High resolution data was collected at pass energy of 5.85 eV with 0.05 eV step sizes and a minimum of 200 scans to improve the signal to noise ratio; lower resolution survey scans were collected at pass energy of 93.5 eV with 0.5 eV step sizes and a minimum of 25 scans. The energies associated with each spectra were calibrated to the C1S (284.6 eV), which corresponds mainly to the carbon black in the composite electrode and adventitious carbon. The data was analyzed using the software CasaXPS and all peaks were fit using a Shirley-type background. Powder and thin film samples were disassembled in an Ar-filled glove box, washed with solvent three times, dried and then transferred to the XPS without exposure to the air using a specialized loadlock system.

*Electrochemistry.*—The electrochemical properties of the power electrodes were measured using 2016 coin cells consisting of metallic lithium as an anode and an electrolyte comprised of 1M $LiPF_6$ in a 1:1 volume fraction of ethylene carbonate (EC)/dimethyl carbonate

* Electrochemical Society Student Member.
** Electrochemical Society Active Member.
z E-mail: shmeng@ucsd.edu

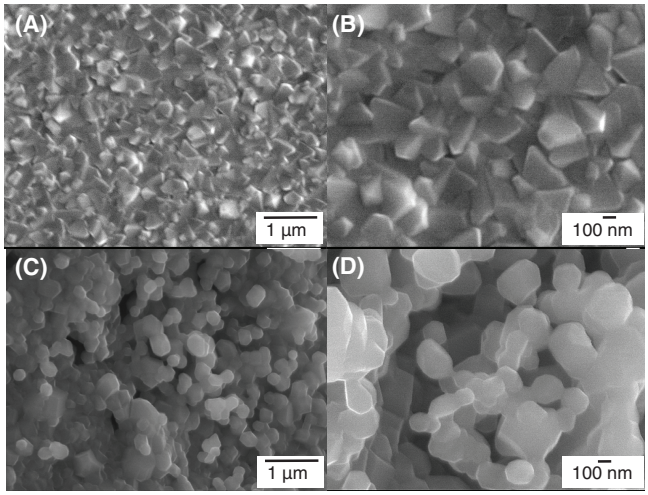


**Figure 1.** SEM images of thin film (A, B) and powder (C, D) MnNi spinel electrode materials.

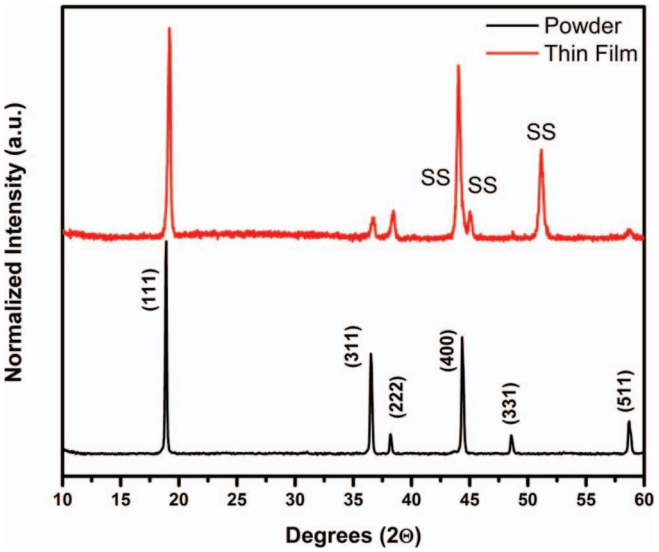


**Figure 2.** XRD patterns for both thin film (top) and powder composite (bottom) MnNi spinel electrodes prior to electrochemical cycling.

(DMC). Celgard type C480 (CelgardInc.USA) was used as separator. Cathode films were prepared from slurries of $LiMn_{2-x}Ni_xO_{4-\delta}$ powders with 7.5% PVdF and 7.5% acetylene carbon black dissolved in N-methyl-2-pyrrolidinone (NMP). The mixtures were cast onto Al foil using a doctor blade and dried at 100°C overnight. Electrode disks were cut into cathodes containing 2–3 mg of active material before storing them in an argon-filled glove box ($H_2O$ level<2 ppm). The coin-cells were assembled in an argon filled glove box and tested using an Arbin BT2000 instrument in galvanostatic mode. The tests were conducted between 5 V and 3.6 V at a constant current rate of C/20. The electrochemical properties of cathode thin film was measured using Swagelok type cell consisting of metallic lithium as an anode, an electrolyte comprised of 1M $LiPF_6$ in a 1:1 volume fraction of ethylene carbonate (EC)/dimethyl carbonate (DMC) and Celgard type C480 separator (CelgardInc.USA). The Swagelok cells were assembled in an Ar-filled glove box and tested using an Arbin BT2000 instrument in galvanostatic mode. The tests were conducted between 5 V and 3.6 V at a constant current rate of C/20.

## Results and Discussion

SEM images of both the powder and thin film samples are shown in Figure 1. Formation of the spinel structure at 600°C using the PLD method shows a dense yet relatively faceted crystal morphology with well-defined grains ranging between 100–200 nm. The grains exhibited an octahedral-type morphology reflecting the cubic spinel structure. Compared to the PLD method, the sol-gel synthesis produced 100 nm particles with a pseudo-polyhedral morphology when calcinated at 800°C. Figure 2 shows the XRD patterns for the MnNi spinel thin film deposited on a SS substrate at 600°C and the sol-gel synthesized powder. All diffraction peaks from the thin film electrode can be indexed to the spinel structure with an Fd-3m space group and the SS substrate. A (111) textured structure is observed for the thin film, as evidenced by the XRD pattern, resulting in larger relative intensities for the (111)/(311) and (111)/(222) peaks compared to that of the synthesized MnNi spinel powder material. Rietveld refinement on the powder material similarly shows the disordered Fd-3m space group with no NiO impurities (see supporting information).[18,19] The refinement results show a lattice parameter of 8.1804 Å, consistent with previously published data.[20,21] For the disordered (Fd-3m) structure both the $Mn^{4+}$ and $Ni^{2+}$ ions occupy the octahedral 16(d) sites. In addition, the disordered structure exhibits the formation of $Mn^{3+}$ ions as a result of oxygen vacancies, which offers improved performance due to an enhancement in electronic conductivity, relative to the ordered ($P4_332$) structure.[21]

The electrochemical properties of the MnNi spinel powder and thin film were investigated in lithium half-cells. The charge/discharge profiles between 3.6 and 5.0 V are shown in Figure 3a and 3c. The MnNi spinel powder and thin film electrodes have a reversible capacity of ~130 mAh/g and ~125 mAh/g, respectively. In addition, both cells have two distinct voltage plateaus around 4.7 V, which corresponds to the $Ni^{2+}$-$Ni^{4+}$ redox couples. A relatively smaller plateau can be found in the 4.0 V region for the thin film material during the first charge cycle corresponding to the $Mn^{3+}$-$Mn^{4+}$ redox couple. The high vacuum deposition process of the PLD system may cause oxygen loss and can lower the average oxidation state of Mn and introduce more $Mn^{3+}$ surface ions. The lower deposition temperature associated with the thin film process may also be attributed to the lower reversible capacity compared to the powder electrodes. To study the rate capability of the MnNi spinel electrodes, half-cells were charged to 5.0 V at a constant current density (C/20) and discharged to 3.6 V at various current densities. The measured discharge capacities with the various current densities are shown in Figure 3b and 3d. When the rate increases from C/20 to 2C for the thin film electrodes only a relatively small capacity loss (~15%) is shown. In contrast, the composite electrode shows a capacity loss of ~40%. The rate capability results of the thin film electrode in the absence of carbon black and binder indicates the intrinsically fast Li diffusion in the MnNi spinel material due to the 3D Li-ion diffusion pathway. Variation of the specific discharge capacity with respect to the cycle number at a constant current density (C/20) shows little capacity fading after 5 cycles for both composite and thin film electrodes (see supporting information).[19]

X-ray photoelectron spectroscopy was used to examine surface features of the thin film and powder electrode materials after electrochemical cycling. The thin film batteries were disassembled, in the fully discharged state, in an argon-filled glove box and transferred to the XPS using a load-lock system to eliminate exposure to air. Figure 4 shows the spectra observed for the C1s, Ni2p, and P2p regions for pristine and cycled samples. The thin film electrodes offer the ability to probe the surface of the cathode material more accurately than that of the composite powder electrodes. This is critically important when trying to determine failure mechanisms associated with the cathode material. For example, the thin film electrodes show no significant formation of decomposed electrolyte such as the formation of carbonate species after electrochemical cycling, evident in the C1s data (Fig 4d). This suggests that even at the higher voltages (5 V) during charging, the MnNi spinel material is intrinsically stable and does not contribute to the decomposition of the electrolyte. In contrast, the

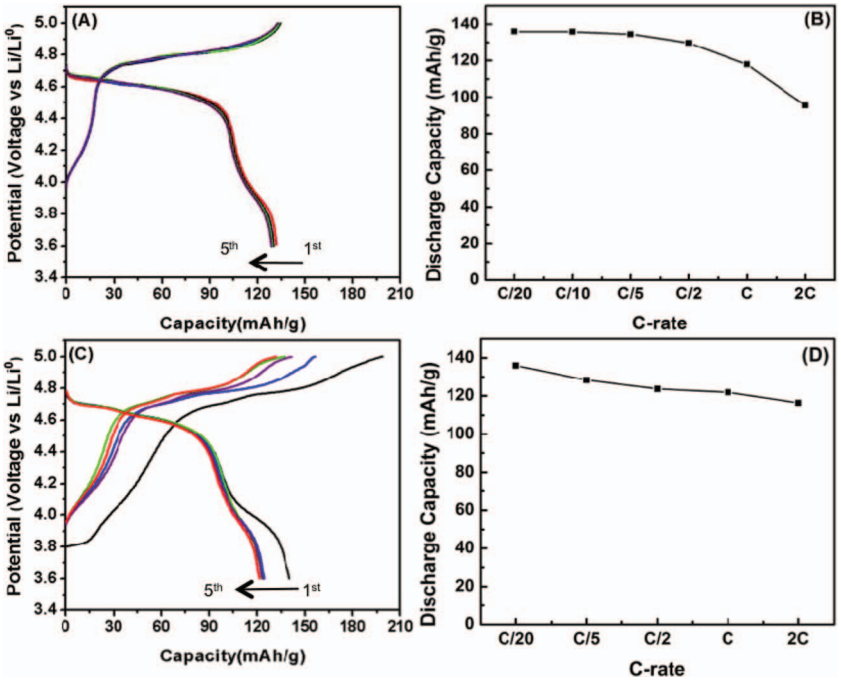


**Figure 3.** Charge/discharge profiles and rate testing for MnNi spinel powder (A, B) and thin film (C, D) electrodes.

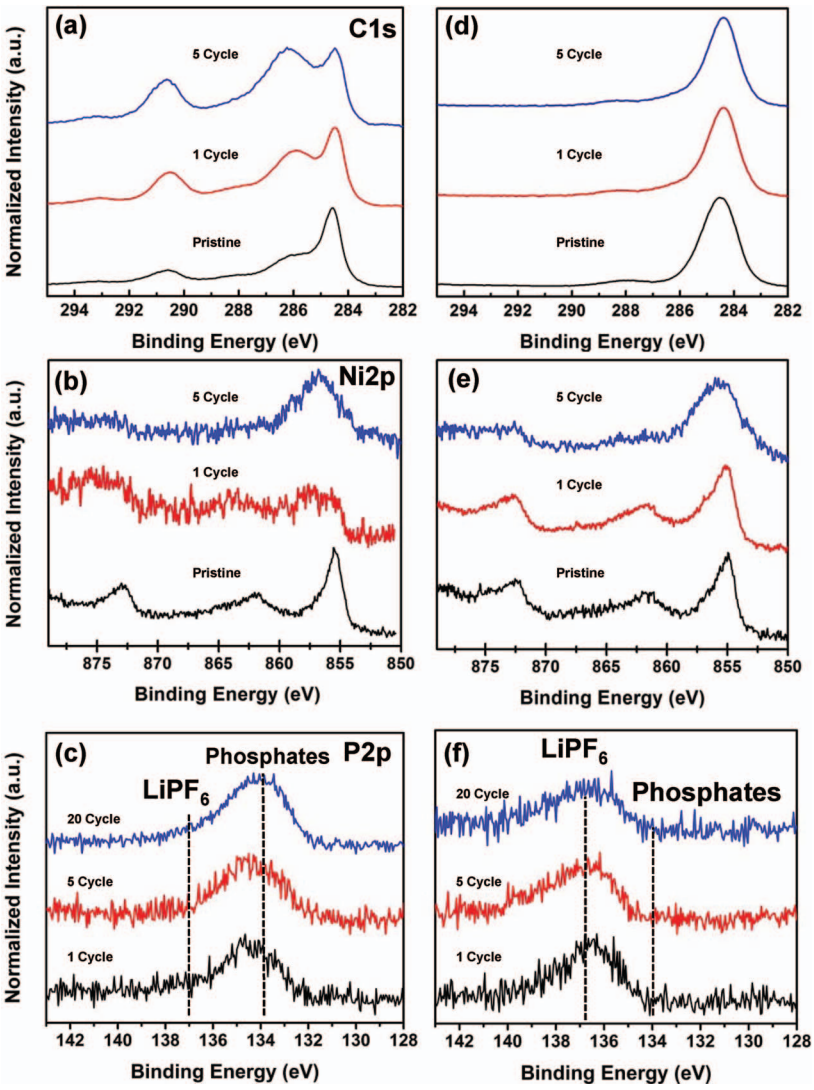


**Figure 4.** XPS data collected using a Mg anode on pristine and post electrochemically cycled powder composite (a–c) and thin film (d–f) MnNi spinel electrodes.

composite electrode shows several peaks, which are associated with the carbon additive and PVdF binder (Figure 4a). The C1s spectra can be de-convoluted into 4 peaks. The peak at ∼284.6 eV (C-C, C-H) corresponds mainly to carbon black while the peaks at 285 eV (-$CH_2$-), and 290.5 eV ($CF_2$) correspond to the PVdF binder.[22] A peak at 287 eV (C-O) corresponds to the EC/DMC electrolyte. The powder composite electrodes shown a gradual increase in the C-O peak with increasing cycle numbers corresponding to the decomposition of the ethylene carbonate and dimethylene carbonate (EC/DMC) electrolyte solution. In addition, the O1s spectra for the composite electrodes show the gradual formation of a C-O (∼533 eV) species after cycling consistent with the C1s spectra for the decomposition of the EC/DMC electrolyte during cycling (see supporting information).[19] In contrast, no C-O formation is seen for the thin film electrode after extended cycling.

Changes can also be seen in the Ni2p region where a significant loss of spectral features, particularly a loss in intensity and peak shape, are present for the composite electrode (Figure 4b). This can be attributed to a large signal from the carbon black and PVdF binder and a relatively lower stoichiometry when compared to Mn in the spinel structure, resulting in a lower percentage of surface exposed Ni. Loss of spectral intensity detracts from adequately assessing the effect cycling on the surface of the MnNi spinel material. The Ni2p region scans for the thin film, however, have a much higher signal-to-noise ratio than those of the composite electrode due to the elimination of carbon black and PVdF binder (Fig. 4e). The Ni2p region shows a slight loss in spectral resolution and broadening of the $Ni2p_{3/2}$ peak upon extended cycling. It is hypothesized that this may be contributed to a higher nickel valence ($Ni^{3+}/Ni^{4+}$) and suggests some irreversibility of the surface Ni species, which contributes little to the total capacity. De-convolution of the Mn $2p_{3/2}$ spectra (see supporting information) for the thin film and composite electrodes reveals two peaks, a minor peak at 641.2 eV ($Mn^{3+}$) and major peak at 642.5 eV ($Mn^{4+}$) confirming the presence of a small amount of $Mn^{3+}$, similar to previous reports by Shaju et al.[19,23,24]

The F1s and P2p region scans offer the most contrast between the thin film and composite electrodes for the formation of the SEI layer. It has been reported for composite electrodes, $LiPF_6$ will react and form LiF and $PF_5$ as byproducts, which further reacts with water forming $POF_3$ and HF on the surface of the particles.[16] This trend is consistent with our composite electrodes, which show the presence of phosphates after electrochemical cycling, shown in the P2p and F1s spectra (Figure 4c and Figure S3 in the supporting information).[19] However, in the thin film XPS analysis, no phosphate formation is shown and only a small amount (<5%) of LiF after 20 cycles, which suggests minimal electrolyte decomposition on the surface of the electrode after extended cycling.

The results from this analysis implies that the surface of the MnNi spinel material is not directly contributing to the SEI formation mechanism; rather the SEI formation seen in the composite electrodes is a result of the incorporation of carbon black and PVdF. These results may also explain the enhancement seen in the rate testing for the thin film electrodes relative to the composite electrode, which enables fasters Li mobility without the formation of an SEI layer and without the inactive PVdF binder.

## Conclusions

This work, through the surface characterization of both composite and thin film electrodes, provides evidence of the intrinsic stability of the MnNi spinel material. The existence of no oxidized $POF_3$ and only minimal LiF formation on the surface of the thin film electrodes after extended cycling shows its ability to withstand the stress of higher operating voltages. Work is currently being conducted to model the electrolyte/electrode interface to more systematically investigate the role the MnNi spinel plays at these higher operating voltages. In addition, this study provides evidence that more research needs to be dedicated to either finding polymer binders that do not play a role in the formation of an SEI layer or more research into implementing thin film electrodes for commercial applications.

## Acknowledgments

YSM and KJC acknowledge the support from the U.S. Department of Energy, Office of Basic Energy Sciences under Award Number DESC0002357. NJD acknowledges the support from the Fluid Interface Reactions, Structures and Transport (FIRST) Center, an Energy Frontier Research Centers funded by the U.S. Department of Energy, Office of Science, Office of Basic Energy Sciences (Award Number ERKCC61). MCY acknowledges the final support from Florida Energy System Consortium (FESC). A portion of this work was also supported by the U.S. Department of Energy's Office of Basic Energy Science, Division of Materials Sciences and Engineering, under contract with UT-Battelle, LLC. (GMV). MCY thanks the Major Analytical Instrumentation Center (MAIC) at the University of Florida.

## References

1. Y. Talyosef, B. Markovsky, R. Lavi, G. Salitra, D. Aurbach, D. Kovacheva, M. Gorova, E. Zhecheva, and R. Stoyanova, *J. Electrochem. Soc.*, **7**, 154 (2007).
2. A. M. Andersson, D. P. Abraham, R. Haasch, S. MacLaren, J. Liu, and K. Amine, *J. Electrochem. Soc.*, **10**, 149 (2002).
3. D. Aurbach, B. Markovsky, G. Salitra, E. Markevich, Y. Talyossef, M. Koltypin, L. Nazar, B. Ellis, and D. Kovacheva, *J. Power Sources*, **2**, 165 (2007).
4. D. Aurbach, I. Weissman, A. Schechter, and H. Cohen, *Langmuir*, **16**, 12 (1996).
5. D. Ostrovsky, F. Ronci, B. Scrosati, and P. Jacobsson, *J. Power Sources*, 94 (2001).
6. A. Schechter, D. Aurbach, and H. Cohen, *Langmuir*, **9**, 15 (1999).
7. L. Dahéron, R. Dedryvère, H. Martinez, M. Ménétrier, C. Denage, C. Delmas, and D. Gonbeau, *Chem. Mater.*, **2**, 20 (2007).
8. L. M. Bull, B. Bussemer, T. Anupold, A. Reinhold, A. Samoson, J. Sauer, A. K. Cheetham, and R. Dupree, *J. Am. Chem. Soc.*, 122 (2000).
9. R. Dedryvère, S. Laruelle, S. Grugeon, P. Poizot, D. Gonbeau, and J. M. Tarascon, *Chem. Mater.*, **6**, 16 (2004).
10. R. Dedryvère, H. Martinez, S. Leroy, D. Lemordant, F. Bonhomme, P. Biensan, and D. Gonbeau, *J. Power Sources*, **2**, 174 (2007).
11. A. P. Grosvenor, M. C. Biesinger, R. S. C. Smart, and N. S. McIntyre, *Surf. Sci.*, **9**, 600 (2006).
12. S. Leroy, H. Martinez, R. Dedryvère, D. Lemordant, and D. Gonbeau, *Appl. Surf. Sci.*, **11**, 253 (2007).
13. K. M. Shaju, G. V. Subba Rao, and B. V. R. Chowdari, *Electrochim. Acta*, **11**, 48 (2003).
14. N. Sharma, K. M. Shaju, G. V. S. Rao, and B. V. R. Chowdari, *J. Power Sources*, **1–2**, 139 (2005).
15. C. Wu, F. Wu, L. Chen, and X. Huang, *Solid State Ionics*, 152 (2002).
16. K. Edström, T. Gustafsson, and J. O. Thomas, *Electrochim. Acta*, **2–3**, 50 (2004).
17. H. Xia, Y. S. Meng, M. O. Lai, and L. Lu, *J. Electrochem. Soc.*, **3**, 157 (2010).
18. M.-C. Yang, B. Xu, J.-H. Cheng, C.-J. Pan, B.-J. Hwang, and Y. S. Meng, *Chem. Mater.*, **11**, 23 (2011).
19. See supplementary material at http://dx.doi.org/10.1149/2.008206esl for XPS, XRD, and rate testing images.
20. T. Ohzuku, S. Takeda, and M. Iwanaga, *J. Power Sources*, 81 (1999).
21. M. Kunduraci, J. F. Al-Sharab, and G. G. Amatucci, *Chem. Mater.*, **15**, 18 (2006).
22. N. Yabuuchi, Y.-C. Lu, A. N. Mansour, S. Chen, and Y. Shao-Horn, *J. Electrochem. Soc.*, **2**, 158 (2011).
23. K. M. Shaju, G. V. Subba Rao, and B. V. R. Chowdari, *Solid State Ionics*, 152 (2002).
24. K. M. Shaju, G. V. Subba Rao, and B. V. R. Chowdari, *Electrochim. Acta*, **2**, 48 (2002).